Korean Journal of Chemical Engineering (2024) 41:729–747
https://doi.org/10.1007/s11814-024-00077-6

ORIGINAL ARTICLE

CFD Study and RSM Optimization of Acetylene Production in Partial Oxidation Process

Maliheh Saravani Ghayour[1] · Seyed Reza Shabanian[1]

Received: 21 April 2023 / Revised: 1 August 2023 / Accepted: 28 August 2023 / Published online: 15 February 2024

Abstract

The present study aims to increase the selectivity of C_2H_2 in the partial oxidation process of methane, employing design of experiments (DOE) and computational fluid dynamics (CFD). Central composite design is used to design tests, and analysis of variance is performed to evaluate the percentage of contribution of operating factors on system performance. The operating factors considered in the analysis are preheating temperature, O_2/CH_4 ratio, and inlet velocity. The system responses are selectivity of C_2H_2 and conversion of CH_4. Furthermore, an optimization method using response surface methodology is utilized to determine the optimal values of operating factors that lead to the best system performance. The findings indicate that increasing the preheating temperature and O_2/CH_4 ratio boosts the selectivity of C_2H_2 and reduces the methane conversion percentage, while increasing the inlet velocity has the opposite effect. The optimization method indicates that the maximum selectivity of C_2H_2 is achieved with conversion of CH_4 of 95% under optimal conditions, namely preheating temperature of 1151.13 K, inlet velocity of 222.8 m/s, and O_2/CH_4 ratio of 0.59.

Keywords Partial oxidation · CFD · Optimization · Acetylene production · RSM

Abbreviations

ANOVA	Analysis of Variance
CCD	Central composite design
CFD	Computational fluid dynamics
DNS	Direct numerical simulation
DO	Discrete ordinate
DOE	Design of experiments
DJHC	Delft-jet-in-hot-coflow
EDC	Eddy dissipation concept
LES	Large eddy simulation
MILD	Moderate or intense low-oxygen dilution
PDF	Probability density function
POX	Partial oxidation
RANS	Reynolds-averaged Navier–Stokes
RSM	Response surface methodology

List of Symbols

E	Total specific energy (j/kg)
H	Coefficient of convective heat transfer (w/m^2 k)
$\vec{J}_j$	Diffusion flux of species j
K	Turbulent kinetic energy
K_{eff}	Effective thermal conductivity
ni	Number of moles of specie i
P	Pressure (pa)
S_h	Reactive radiation source
T	Time (s)
T	Temperature (K)
$\vec{V}$	Velocity vector
xi	Number of carbon atoms in specie i
Y_j	Mass fraction of specie j

Greek Symbols

M	Viscosity (pa s)
P	Density (kg/m^3)
ε	Turbulent dissipation rate
τ_{eff}	Effective shear stress

Introduction

Acetylene plays a vital role in various industrial processes that yield crucial chemicals, such as vinyl acetate, 1,4-butanediol, and polyvinyl alcohol. As crude oil deposits continue to deplete and high oil prices increase pressure on naphtha-derived olefins production, the subject of acetylene production from natural gas is regaining attention. This long-overlooked area of research is now being explored as a potential

✉ Seyed Reza Shabanian
Shabanian@nit.ac.ir

[1] Department of Chemical Engineering, Babol Noshirvani University of Technology, Babol 4714871167, Iran

solution to these challenges [1]. Acetylene can be generated through thermal cracking of hydrocarbon species, partial oxidation or non-partial oxidation, hydration of calcium carbide, and other processes [2]. The most effective way to produce acetylene can differ from one region to another, depending on the varying costs of the raw materials used for its production [3]. Among these, The Partial Oxidation (POX) process of natural gas is the favored acetylene production method in areas with abundant natural gas [4, 5]. The POX process utilizes the energy from burning hydrocarbons with oxygen to pyrolyze residual hydrocarbons and produce acetylene. During this process, acetylene serves as a reaction intermediate, and the gas mixture must be rapidly cooled at the point of optimal acetylene yield [6].

Designing and optimizing the POX process requires conducting extensive experimental studies covering a broad range of operating conditions and mixture compositions. Achieving the optimal design and optimization of the POX process necessitates conducting extensive experimental studies across a wide range of operating conditions and mixture compositions. However, numerical simulations can offer more detailed information and uncover complex interactions between chemical and physical processes, while simultaneously saving significant costs and time compared to experimental studies [2].

Computational fluid dynamics (CFD) is a scientific field that comprehends the non-linear interaction between turbulent flow and chemical reactions, thus enabling the provision of more precise descriptions of the POX process. Also, CFD simulations provide detailed flow field and species concentration profiles, which are crucial pieces of information for reactor design and optimization. Furthermore, the use of computational fluid dynamics modeling allows for flexibility in adjusting design parameters without incurring the costs associated with modifying research equipment. This leads to significant cost savings and time efficiency [7–9]. Currently, Direct Numerical Simulation (DNS) is exclusively utilized for small-scale and low Reynolds-number flows due to its substantial computational cost [10, 11]. In research, Large Eddy Simulation (LES) has become increasingly prevalent, yet its application to industrial reactors remains cost-prohibitive. In contrast, Reynolds-Averaged Navier–Stokes (RANS) simulation offers greater computational efficiency and can reliably predict mean quantities [12, 13]. In the study of turbulent combustion, the Probability Density Function (PDF) [14, 15] And Eddy Dissipation Concept (EDC) [16–19] models are extensively employed in the calculation of finite-reaction rate in flames. The EDC has found widespread usage in the industry for the numerical simulation of turbulent combustion problems over the past three decades.

Evan et al. used an optimized EDC model to simulate the lifted jet flames in a heated coflow. The simulation results showed good agreement with the measured temperature, as well as concentrations of hydroxyl (OH) and formaldehyde (CH_2O) [19]. De et al. examined the interaction between turbulence and chemistry using the EDC model for the Delft-Jet-in-Hot-Coflow (DJHC) flames. Their main focus was on evaluating the EDC model's performance when used with two-equation turbulence models and chemical kinetic schemes. They observed that the EDC model accurately predicted the experimentally observed trend of lift-off height variation with jet Reynolds-number [20]. Xu et al. conducted a simulation study of the POX reformer utilizing modified EDC and PDF models. The investigation focused on the impact of operating pressure parameters, O_2/NG ratio, and Steam/NG ratio on the performance of the reformer. The findings indicated that the modified EDC model outperformed the PDF model. Furthermore, the study revealed that an increase in pressure augmented conversion of CH_4, whereas an increase in O_2/NG ratio resulted in an elevation of temperature [21]. Zhang et al. utilized the EDC model in CFD, which was coupled with detailed chemistry, to simulate the JICF reactor for conversion of CH_4 to acetylene in a Partially Decoupled Process (PDP) [22]. Using experimental data, Chen conducted a numerical simulation of the combustion reaction of natural gas in a reactor that included a mixer. The simulation revealed that delayed mixing resulted in a decrease in the yield of C2 and a higher conversion of CH_4 to CO [23]. Zhou et al. [24] conducted a 3D simulation of the NC-POX process of natural gas in a high-pressure reformer. They investigated how the pressure parameters, O_2/CH_4 ratio, and O_2/H_2O ratio affect the performance of syngas using the GRI Mesh3.0 mechanism. Amirshaghaghi et al. [25] used the CFD method to simulate the partial oxidation of methane in an autothermal reactor's combustion chamber. The simulation results revealed that increasing the O_2/CH4 ratio from 0.5 to 0.8 caused a 15.4% decrease in the H_2/CO ratio and a 42.7% decrease in CH_4 conversion. Zhou et al. [26] executed an assessment of three mechanisms—GRI-Mech 3.0, Konnov 0.5, and Petersen C5_44 for the oxidation of $CH_4/C_2H_6/C_3H_8$/air mixtures under high-pressure and high-temperature conditions. They analyzed the impact of initial O_2/CH_4 and O_2/H_2O ratios, operating temperature, and pressure on the ignition and reforming reactions in an industrial reformer using a series of simulations. The results indicated that the GRI-Mech-3.0 model was the most effective. In addition, the study revealed that the conversion of methane necessitates a minimum O_2/CH_4 ratio under high pressure and temperature, and the addition of H_2O can regulate the H_2/CO ratio and flame temperature. Hosseini et al. [27] conducted research on the characteristics of flameless combustion of biogas using a three-dimensional CFD model. They utilized a two-stage mechanism, an eddy dissipation model, and the standard k-ε turbulence model. The study focused on the impact of preheated and wall temperature on the reaction zone and the formation of pollutants. According

to the results, while conventional combustion with preheated biogas resulted in lower fuel consumption, it also led to increased formation of NO_x. Shabanian et al. [28] developed a CFD model to predict NO_x emissions, temperatures, and species mole fractions in a MILD combustion burner. For the simulations, they employed three turbulence models along with two kinetic mechanisms and three combustion models. The study revealed that the KPP and CFD results exhibited strong agreement with experimental observations only when incorporating the RSM-transition turbulence model, along with the modified EDC and POLIMI 1101 syngas mechanism in the model. Jeon et al. [29] studied how the fuel–air injection rate and fuel-to-air ratio affect Moderate Or Intense Low-Oxygen Dilution (MILD) combustion using a two-dimensional simulation of non-catalytic partial oxidation in a cylindrical furnace. They found that reducing the fuel–air injection rate led to a higher temperature peak during combustion and that a lower O_2/CH_4 ratio resulted in longer jet penetration and higher H_2/CO ratio in the outflow. Kertthong et al. [30] conducted research on the utilization of non-catalytic partial oxidation of methane in high-steam biomass-derived syngas to maximizing CH_4 conversion and the production of desirable gases (H_2 and CO) for synthesis applications. The study focused on examining the impact of oxygen-to-fuel ratio, steam, and preheating temperature on the process. Lim et al. [31]. proposed a partial oxidation compression ignition reformer for synthesizing gas from methane. They examined the impact of variables such as the O_2/CH_4 ratio, the overall flow rate, the temperature of the preheated intake, and the ratio of oxygen enrichment in order to identify the most favorable conditions. The results showed that increasing the O_2/CH_4 ratio and total gas flow led to a rise in the concentration of the synthesis gas, which then reached its maximum value before decreasing. Additionally, the synthesis gas yield increased proportionally with the intake preheating temperature and oxygen enrichment ratio.

The geometry of a combustion chamber and varying configurations of the nozzle utilized can significantly affect the stability and efficiency of combustion inside a combustion chamber and the concentration of various components in the product stream [32–34]. The design of the chamber can impact the mixing of fuel and oxidizer, the residence time of reactants, and heat transfer within the chamber, all of which can influence the combustion process. Numerous researchers have conducted both numerical and experimental studies to investigate the respective effects of combustor shape and dimensions on combustion and emission [35–46]. The following described some of the literature: Tu et al. conducted a numerical investigation to analyze how the shape of the furnace chamber in an industrial-scale furnace operating under MILD conditions affects the combustion of natural gas. They varied the angle α between the furnace roof and sidewall from 80° to 100° to alter the shape of the chamber. Their findings demonstrated that increasing the α angle resulted in a more robust recirculation flow field with more combustion products in the reactants, lower peak temperatures, and reduced NO_x emissions [35]. Deng et al. conducted a numerical investigation to analyze how the combustion characteristics of methane fuel are affected by different nozzle configurations. Their findings indicated that increasing the number of nozzles led to a decrease in the low-temperature zone and an increase in the maximum temperature [37]. Mendoza et al. studied the impact of coolant types and reactor diameter on the performance of a tubular reactor that employs CFD modeling for oxidative dehydrogenation of butene. The research showed that increasing the reactor diameter caused a rise in temperature gradient, but a decline in yield and conversion. overall, using a smaller diameter and solar salt as a coolant can boost reactor performance and cut down the overall costs linked to separation and treatment systems [40]. Chmielewski et al. conducted experimental and numerical studies on a novel variable geometry combustor for a miniature gas turbine. Their aim was to improve combustion efficiency and reduce NO_x and CO emissions across a broad range of operating conditions. The experimental results showed a 40% reduction in NO_x and a twofold decrease in CO emissions. Furthermore, there was a strong correlation between the experimental and numerical results [41].

Forster et al. [39] evaluated four different burners (jet, jet-swirl, plate, spherical) numerically (2D and 3D) and experimentally for an HP POX burner. The results found that the plate and spherical burners have a shorter combustion zone due to faster exothermic reactions and higher temperatures. The plate burner showed a more complex interaction with recirculating gas streams, while the spherical burner achieved higher conversion rates compared to the jet configuration. Cheong et al. [42] studied the stability and specifications of non-premixed MILD combustion of propane using a cylindrical furnace with a parallel-jet burner, while avoiding preheating and dilution. the results showed that the spacing between the fuel and air nozzles was a critical factor to consider when designing burners with parallel nozzles.

The integration of CFD simulation with the design of experiments (DOE) has gained attention as an effective method [47]. By combining CFD with DOE, a systematic understanding of the interactions among design and operational variables and their impacts on the entire system can be achieved [48]. This approach has been successful in various engineering fields such as micro-mixers [49, 50], cooling packages [51], and photocatalytic reactors [48, 52]. Furthermore, no attempts have been made to use CFD combined with DOE for multi-objective optimization of POX methane.

The present work a study that examines the effects of preheating temperature, inlet velocity, and the oxygen-to-methane ratio (O_2/CH_4) on acetylene selectivity and conversion of CH_4 in POX process. Alternatively, the shape of

the reactor geometry is investigated as a crucial parameter in the design of reactors. In order to further examine the impact of operating parameters, a methodology combining CFD and DOE was employed to derive equations that accurately describe the selectivity of C_2H_2 and the conversion of CH_4. The optimization of operating conditions is essential in industrial processes, and to achieve this, the DOE optimization method was employed in this study.

Problem Definition

The reactor selected for this study is based on the article by Dongar Chen et al. [43] and consists of four parts, namely: inlet nozzles, oxygen-supply tube, the main reactor body, and outlet. The main reactor chamber has a height of 900 mm and a diameter of 400 mm. The inlet nozzles used for fuel injection are 150 mm in height and 43.3 mm in diameter. Additionally, the oxygen-supply tube, with a diameter of 5 mm and a height of 150 mm, aids in stabilizing the flame. A schematic of the investigated combustion reactor is illustrated in Fig. 1.

Modeling

Governing Equations

The equations governing combustion simulation include the continuity, momentum, energy, and mass conservation equations. To investigate the flow of combustion gases and their effects on heat transfer to reactor tubes, fuel requirements, and other conditions within the combustion chamber, researchers have employed three-dimensional simulations of the chamber using CFD techniques. In gas furnaces where the fluid is compressible, the stable compressible continuity equation is utilized.

$$\frac{\partial \rho}{\partial t} + \vec{\nabla} \cdot \left(\rho \vec{V}\right) = 0 \tag{1}$$

Typically, the momentum equation is analyzed alongside the Reynolds-Averaged Navier–Stokes (RANS) equations:

$$\frac{\partial \rho \vec{V}}{\partial t} + \vec{V} \cdot \vec{\nabla}\left(\rho \vec{V}\right) = -\vec{\nabla} p + \vec{\nabla} \cdot \left(\mu \nabla \vec{V}\right) \tag{2}$$

The energy equation and its details can vary across studies depending on the researchers' approach and the methods and models they employ.

$$\begin{aligned} &\frac{\partial}{\partial t}(\rho E) + \nabla \cdot \left(\vec{V}(\rho E + P)\right) \\ &\quad = \nabla \cdot \left(K_{\text{eff}} \nabla T - \sum_j h_j \vec{J}_j + \left(\tau_{\text{eff}} \cdot \vec{V}\right)\right) + S_h \end{aligned} \tag{3}$$

Equations (1)-(3) consist of variables representing the Velocity Vector (V), Fluid Flow Density (ρ), Flow Viscosity (μ), Flow Pressure (P), Flux Penetration ($\vec{J}$), Effective Thermal Conductivity (K_{eff}), Effective Shear Stress (τ_{eff}) and Reactive Radiation Source (S_h). The mathematical equations presented below describe the total energy and enthalpy effects of ideal gases:

$$E = h - \frac{P}{\rho} + \frac{V^2}{2} \tag{4}$$

$$h = \sum_j Y_j h_j \tag{5}$$

The variable Y_j represents the effect of the mole fraction of species j.

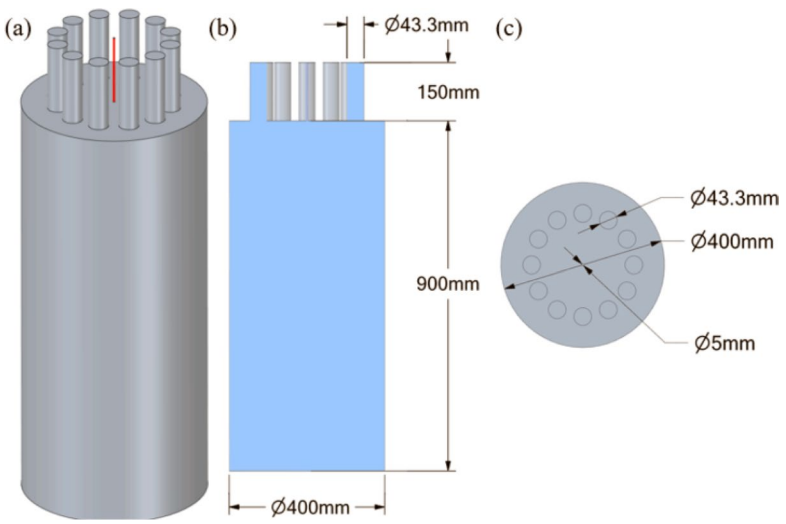

Fig. 1 **a** Structure of reactor (oxygen-supply tube is in red), **b** Side view, and **c** top view

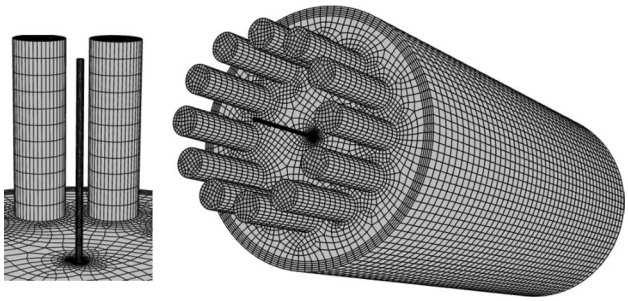

Fig. 2 A view of the circle geometry mesh

Grid-Independence Test

The Ansys Meshing software has been used to perform the meshing process and the simulations have been conducted using Ansys FLUENT 17.2 [53] and the SIMPLE algorithm was used for pressure–velocity relationship. The grid independence test involved evaluating the temperature, C_2H_2, CO, and H_2 mole fractions along the central axis of the reactor. To demonstrate grid dependency, various geometries were examined using different mesh numbers of 51529, 102538, 159159, 179904, and 205372 (Fig. 2). As shown in Figs. 3, 4, 5, 6, there was a negligible variance in the temperature, C_2H_2, CO, and H_2 mole fractions observed in mesh numbers 159159, 179904, and 205372, and no significant discrepancies were found. Therefore, the geometry with mesh number 159159 (Fig. 2) has been selected as the final configuration for all subsequent simulations.

The realizable K-ε model, which has been recognized as the optimal approach for analyzing flow perturbations in the combustion chamber, has been employed alongside the EDC combustion model, chosen for its swift computational performance. For the simulation of Thermal Radiation, the Discrete Ordinate (DO) model has been employed, and the modified GRI 3.0 mechanism (36 chemical components and 219 main reactions) has been utilized to effectively model the chemical interactions of the turbulence.

In Fig. 7, the mole fraction of components that exit the reactor has been depicted using the Modified GRI3.0 [54], Reduced GRI 3.0 [55, 56] mechanisms, and industrial data.

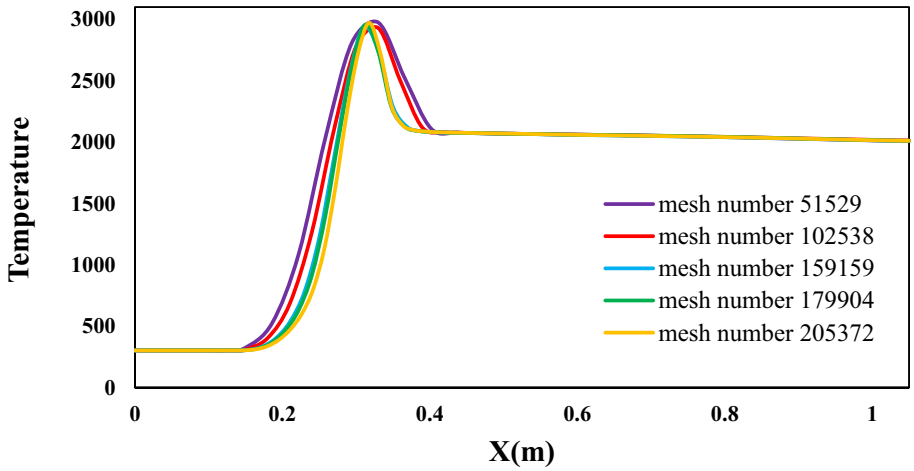

Fig. 3 Comparison of temperature profiles with five different meshes along the central axis

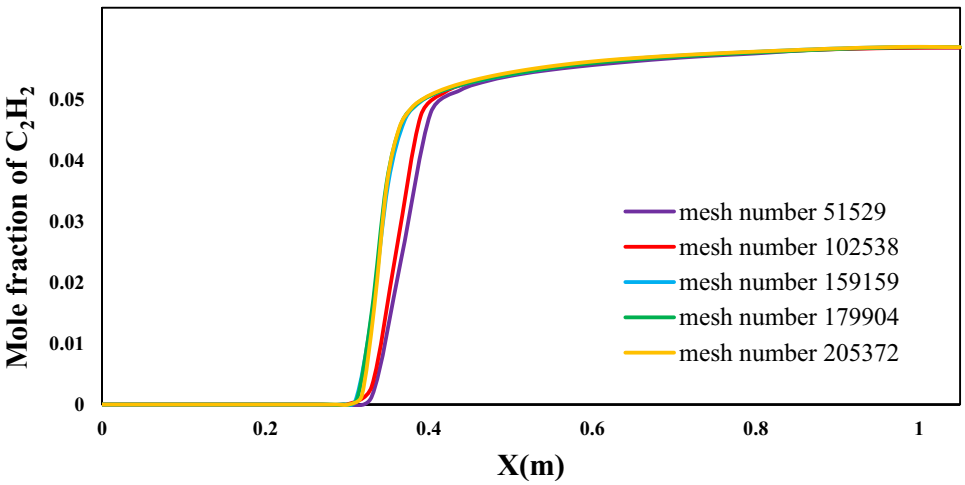

Fig. 4 Comparison of mole fraction of C_2H_2 profiles with five different meshes along the central axis

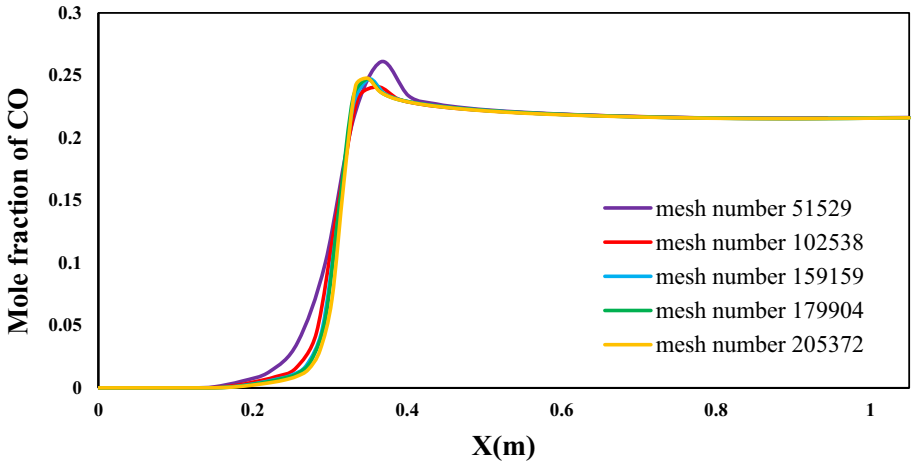

Fig. 5 Comparison of mole fraction of CO profiles with five different meshes along the central axis

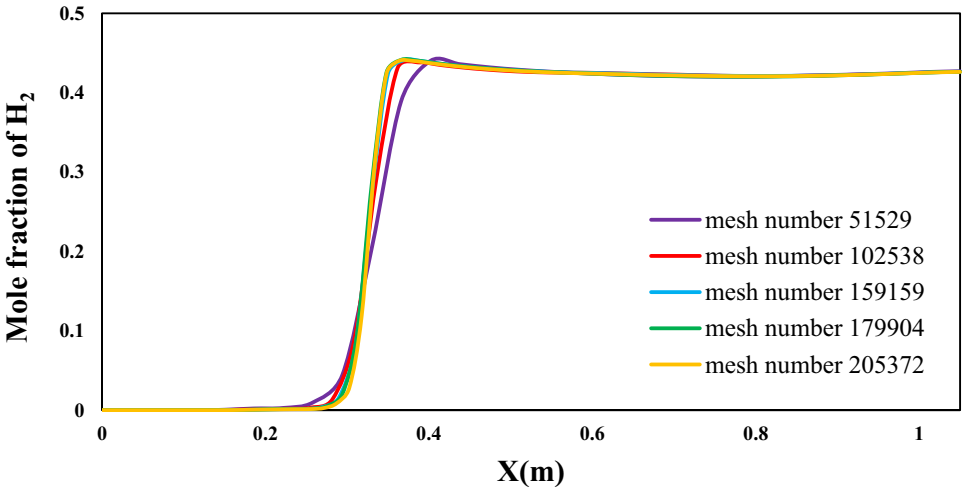

Fig. 6 Comparison of mole fraction of H_2 profiles with five different meshes along the central axis

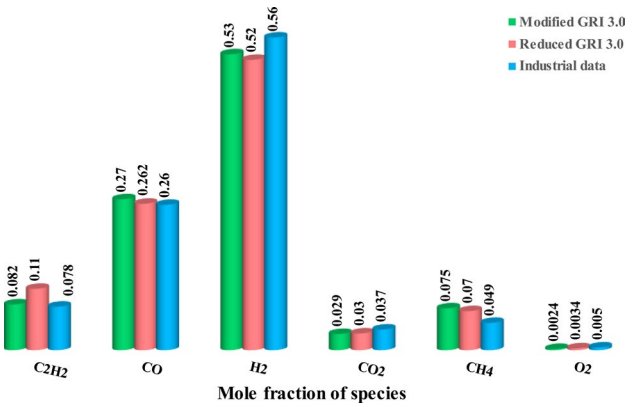

Fig. 7 Comparison of the predicted mole fractions of the main products from two mechanisms, reduced GRI 3.0 and modified GRI 3.0, with experimental data at the reactor outlet

The findings have demonstrated that the simulation conducted with the Modified GRI 3.0 mechanism has been more consistent with the industrial data. Therefore, for subsequent simulations, the Modified GRI mechanism has been chosen to enhance the accuracy and dependability of the simulation model.

Design of Experiments

The Design of Experiments (DOE) is a branch of applied statistics that involves planning, conducting, analyzing, and interpreting predetermined numerical or experimental tests to evaluate the factors that control a parameter or a group of parameters [57]. In this research, DOE is utilized to achieve two objectives: firstly, to reduce computational costs and the number of numerical tests; and secondly, to develop appropriate mathematical models that explain the impact of design variables on each objective function.The test table used in this study is based on Box and Wilson's Central Composite Design (CCD), which is a commonly used experimental design method [58]. The total design points needed for a fully rotatable CCD with uniform

coverage consist of the sum of cube points, axial points, and center points. This can be expressed as follows [59]:

$$N = 2^K + 2K + n, \tag{6}$$

where N is the actual number of experiments, n is a number of repetition and K is the number of different factors. In the standard form of CCD, each factor comprises five levels, namely $-\alpha$, 1, 0, -1, and α. The general formula for selecting α is $(2\ \mathrm{K})^{0.25}$.The overall workflow of DOE and optimization has been depicted in Fig. 8.

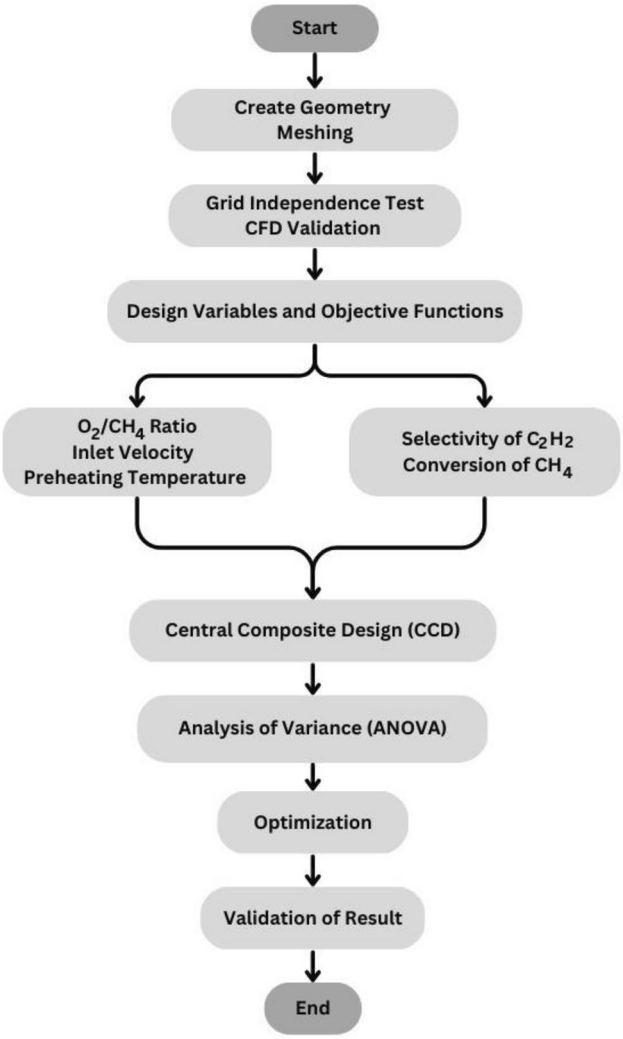

Fig. 8 The flow chart of the simulation and optimization stages

To evaluate the most effective operating conditions for enhancing acetylene production, three parameters have been examined in this study, namely preheating temperature, inlet velocity, and oxygen-to-methane ratio. These parameters have been considered as the design factors for the experiment. By examining the conversion of CH_4 and the selectivity of C_2H_2 as responses to the experiment's design, the behavior of each parameter has been analyzed to determine the optimal value for each. Table 1 outlines the values assigned to each level.

To conduct a more comprehensive analysis of the results, the experiment design has been performed using Design-Expert 13 software. Once the levels were determined, Table 2 have been developed, which included a total of 15 tests.

The results from Table 2, generated by the Design-Expert software, have been entered and solved in the Fluent software environment. The objective has been to achieve the highest possible selectivity of C_2H_2, which has also been dependent on the conversion of CH_4. Based on the executed runs and subsequent analysis, the maximum value of selectivity of C_2H_2 has been obtained from RUN3. Therefore, the contours of RUN3 examine to further analyze the results.

Figure 9a shows the temperature contour in section $x=0$. The maximum temperature inside the chamber, around the oxygen-supply tube, has reached 3020 K due to the high concentration of oxygen in that area, leading to complete combustion of methane. Therefore, the concentration of CO_2 has reached its highest level at this zone (Fig. 9b). Furthermore, the temperature gradually decreases towards the wall. The concentration of CO follows a similar pattern to temperature, peaking around the oxygen-supply tube. As reactants are consumed, CO gradually rises at the inlet tubes flame until it is uniformly mixed (Fig. 9c). Figure 9d and e show the distribution of oxygen and methane concentration follows a similar trend. It is evident that the reaction continues until there is enough oxygen available for the reaction to occur. In the second part of the reactor, where the oxygen concentration has been almost depleted, the reaction ultimately comes to an end. Figure 9f shows the concentration gradually rises in the direction of flow. Towards the end of the reactor, when oxygen is depleted, the species concentration throughout the region stabilizes.

Table 1 Range and level of independent variables for CCD runs

Name	Code	Units	−1.682	−1	0	+1	+1.682
Preheating temperature	A	K	898.85	950	1025	1100	1151.15
Velocity	B	m/s	124.425	150	187.5	225	250.575
O_2/CH_4	C	(%)	0.58954	0.61	0.64	0.67	0.69046

Table 2 Actual values of the variables used to design the experiment

Run	A: preheating temperature (k)	B: velocity (m/s)	C: O_2/CH_4	Conversion of CH_4	Selectivity of C_2H_2
1	950	225	0.67	96.03	17.43
2	1100	225	0.61	94.7	22.69
3	950	225	0.61	91.49	25.91
4	1025	124.425	0.64	96.49	15.075
5	1025	250.575	0.64	94.87	22.11
6	1025	187.5	0.64	95.6	19.57
7	950	150	0.61	93.49	23.64
8	1100	225	0.67	97.66	11.92
9	1025	187.5	0.69046	97.74	10.44
10	1100	150	0.67	98.36	6.89
11	898.85	187.5	0.64	93.59	23.04
12	1151.15	187.5	0.64	97.08	14.76
13	1100	150	0.61	95.83	18.8
14	1025	187.5	0.58954	93.3	25.48
15	950	150	0.67	96.88	13.08

During the acetylene formation pathway, two CH_3 radicals combine to form a C_2H_6 molecule. Subsequently, H atoms are continuously removed from C_2 compounds, dividing the process into two stages with low and high temperatures. At lower temperatures, C_2H_2 formation occurs through the R1 reaction, requiring residual oxygen in the system. At higher temperatures, the R2 reaction takes place, driven by the H radical. The radicals C_2H_3 and C_2H_5 produce stable intermediates through the loss of H atoms. In this reaction, CH is produced but rapidly consumed and transforms into components such as the HCCO radical, which is observed in Fig. 9h.

$$2CH_3 \rightarrow C_2H_6 \xrightarrow{+OH/+H/+CH_3} C_2H_5 \xrightarrow{+O_2} C_2H_4 \xrightarrow{+OH/+CH_3} C_2H_3 \xrightarrow{+O_2} C_2H_2 \quad \text{(R1)}$$

$$2CH_3 \longrightarrow C_2H_6 \underset{-H_2}{\overset{+H}{\longrightarrow}} C_2H_5 \xrightarrow{-H} C_2H_4 \underset{-H_2}{\overset{+H}{\longrightarrow}} C_2H_3 \xrightarrow{-H} C_2H_2 \xrightarrow{+O/+OH} HCCO/CO \quad \text{(R2)}$$

$-H_2$

Results and Discussion

Effect of Geometry

The manner in which fuel and oxygen are introduced into the inlet nozzle and their configuration play a crucial role in determining the combustion regime within the chamber, as well as the concentrations of various components in the product flow. To delve deeper into this matter, we compared the plus arrangement of inlet nozzles in Fig. 10, which employed a mesh count of 137,000, with the original geometry presented in Fig. 2.

The definition of boundary conditions is a crucial component in numerical simulation problems involving fluid flow, as their accurate specification can enhance the precision and speed of the solution. The plus and circle configuration has been governed by certain boundary conditions. The preheating temperature for the inlet tubes has been set at 950 K, while the preheating temperature for the oxygen-supply tube has been set at 303 K. Additionally, the inlet velocity for all tubes has been 150 m/s with the O_2/CH_4 ratio 0.59.

Figure 11 displays the mole fractions of main products at the reactor outlet for the plus and circle configurations. The results indicate that when circle inlet nozzles are used, the output of oxygen and methane is lower, implying that the circle configuration has been more conducive to effective partial oxidation of methane. Additionally, the mole fraction of acetylene output has been higher in the circular reactor.

The temperature distribution contour in the $x=0$ section is displayed in Fig. 12a. It is evident that when the nozzle arrangement is plus, the maximum temperature has been extending along the oxygen-supply tube and to the end of the reactor. This phenomenon has occurred because, in this case, there has been still unreacted methane and oxygen in the reactor due to poor mixing. The issue has been

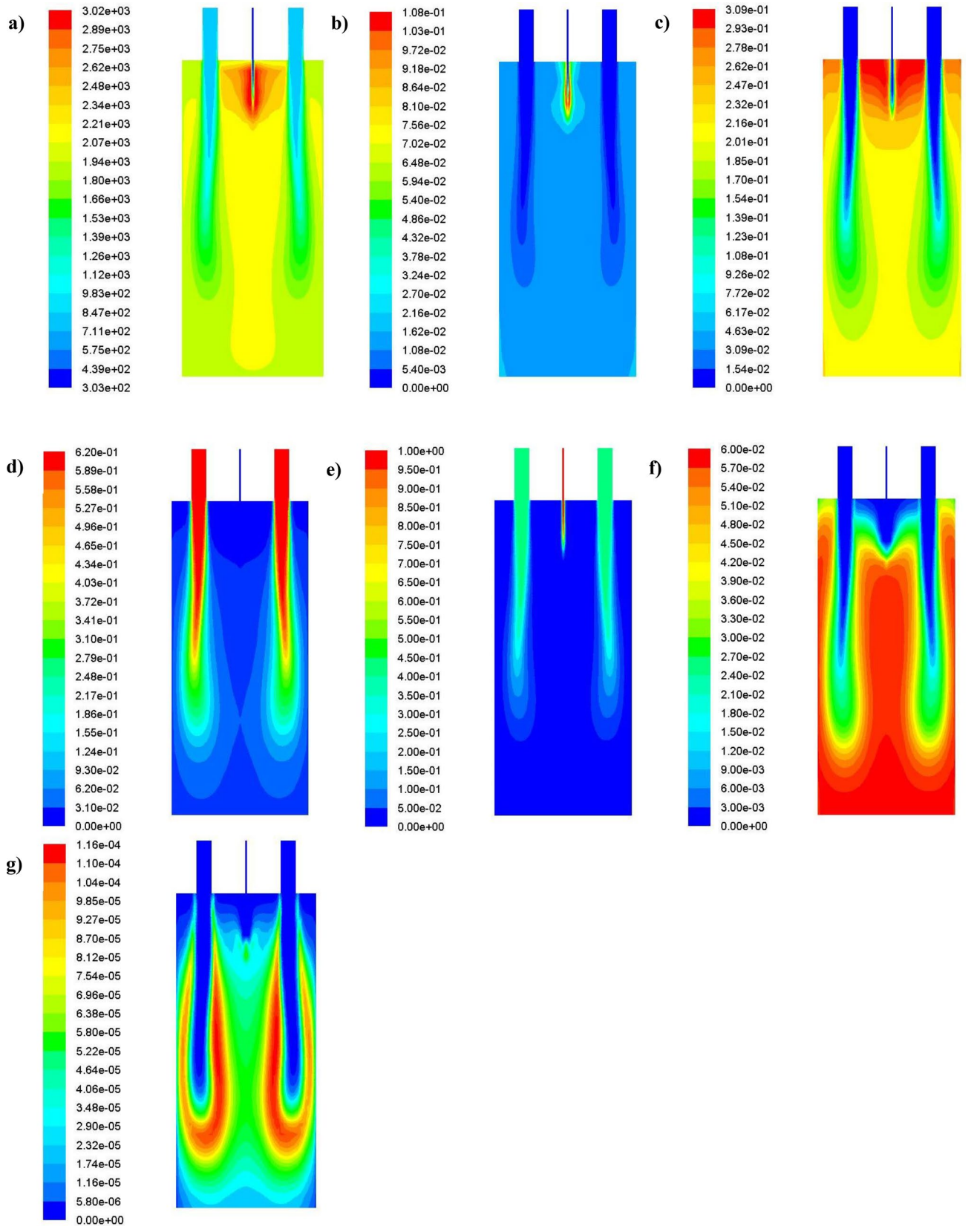

Fig. 9 Contour of reactor YZ section **a** Temperature, **b** mole fraction of CO_2, **c** mole fraction of CO, **d** mole fraction of CH_4, **e** mole fraction of O_2, **f** mole fraction of C_2H_2, **g** mole fraction of HCCO

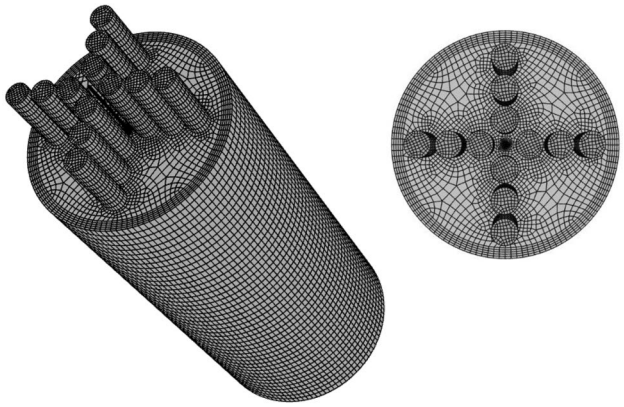

Fig. 10 A view of the PLUS geometry mesh

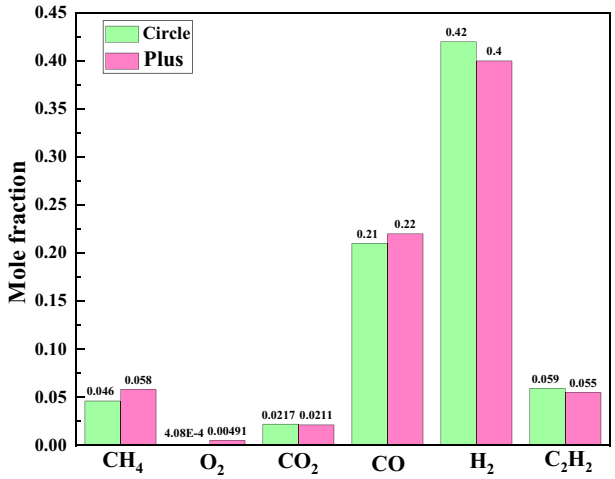

Fig. 11 Mole fractions of main products at the reactor outlet in the circle and plus configuration

further demonstrated in Fig. 12e and f. Similarly, a more uniform distribution within the circular reactor chamber configuration has been illustrated in Fig. 12b–d. Overall, more satisfactory results have been yielded by the circle geometry. Thus, this geometry has been employed in the simulations conducted in this research.

Effect of Increasing Pressure

The effects of increasing pressure at various levels were investigated under a preheating temperature of 950 K, an inlet velocity of 150 m/s, and an O_2/CH_4 ratio of 0.59. As shown in Fig. 13, an increase in pressure from 0.1 to 6 MPa resulted in a decrease of 35.11% in the selectivity of C_2H_2 and a 2.33% decrease in the conversion of CH_4, respectively. These results align with the findings of [24].

Effect of Increasing O_2/CH_4 Ratio

The oxygen-hydrocarbon ratio and preheating temperature of reactants are critical factors in the industrial process of POX natural gas. The following terms, namely oxygen-hydrocarbon ratio, conversion and, selectivity is defined in relation to this process:

$$\text{Oxygen-hydrocarbon ratio} = \left(n(O_2)/n(CH_4)\right) \tag{7}$$

$$\text{Conversion of } CH_4 = \left(n(\text{reacted } CH_4)/n(\text{total } CH_4)\right) \tag{8}$$

$$\text{Selectivity of product} = \left(n_i \times x_i/n(\text{reacted } CH_4)\right), \tag{9}$$

where n is the number of moles, x is the number of carbon atoms in a species, and the subscript i is the name of the species.

Figure 14a displays the conversion of CH_4 at varying ratios. As shown, the conversion of CH_4 has consistently been increasing and has approached 100% as the O_2/CH_4 ratio been increased. The amount of oxygen required for the combustion of methane or natural gas is directly proportional to this ratio. Therefore, a higher O_2/CH_4 ratio has led to a higher conversion rate of CH_4 which is in agreement with the results of Amirshaghaghi et al. [25] and Zhou et al. [26]. This is because a higher ratio enables the combustion of more CH_4, resulting in an increased release of heat, which further raises the conversion rate and outlet temperature.

In contrast to the conversion of CH_4, it is revealed by Fig. 14b that the selectivity of C_2H_2 has been decreasing with an increase in the O_2/CH_4 ratio. For instance, at an O_2/CH_4 ratio of 0.69, the selectivity of C_2H_2 has been reduced to 14.62%, which is lower than the one observed at an O_2/CH_4 ratio of 0.59. This reduction in selectivity has been attributed to the elevated oxidation of CH_4, which has been occurring due to the higher O_2/CH_4 ratio, resulting in a higher production of CO.

Effect of Increasing Preheating Temperature

As shown in Fig. 15a, a higher CH_4 conversion rate has been resulted from an increase in preheating temperature. This effect has been attributed to the increased initial energy in the reaction system, which has promoted a higher rate of CH_4 combustion. As a result, the conversion of CH_4 that has undergone conversion has been significantly increased with a higher preheat temperature. The effect of increasing the preheating temperature on the selectivity of C_2H_2 has been illustrated in Fig. 15b. It has been observed that as the preheating temperature has been increased from 900 to 1150 K, the selectivity of C_2H_2 has been reduced by 25.38%.

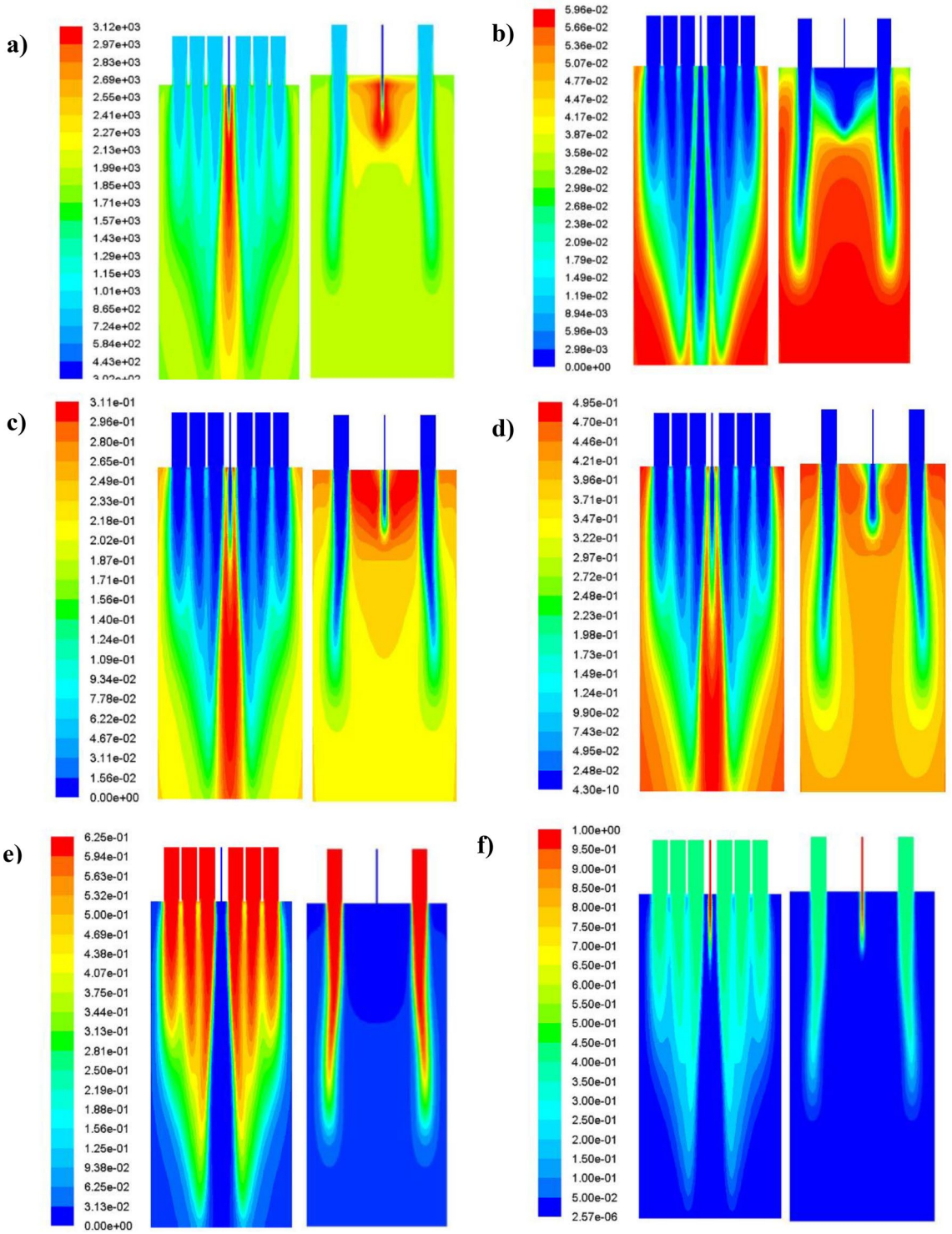

Fig. 12 Contour of reactor YZ section **a** Temperature, **b** mole fraction of C_2H_2, **c** mole fraction of CO, **d** mole fraction of H_2, **e** mole fraction of CH_4, **f** mole fraction of O_2

Effect of Increasing Inlet Velocity

The effect of inlet velocity on the reaction has been conducted under the conditions of constant preheating temperature and constant ratio of O_2/CH_4, in the range of 120–220 m/s. Figure 16a illustrates that the conversion of CH_4 has been decreasing due to the reduction in residence time, as the velocity has been increasing. Figure 16b

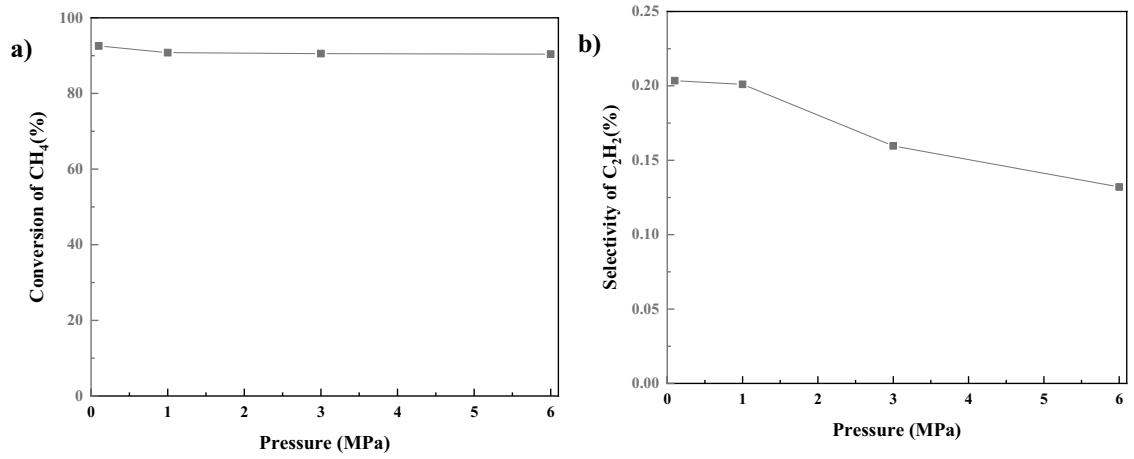

Fig. 13 The effect of increasing pressure on **a** the percentage conversion of CH_4, **b** the selectivity of C_2H_2

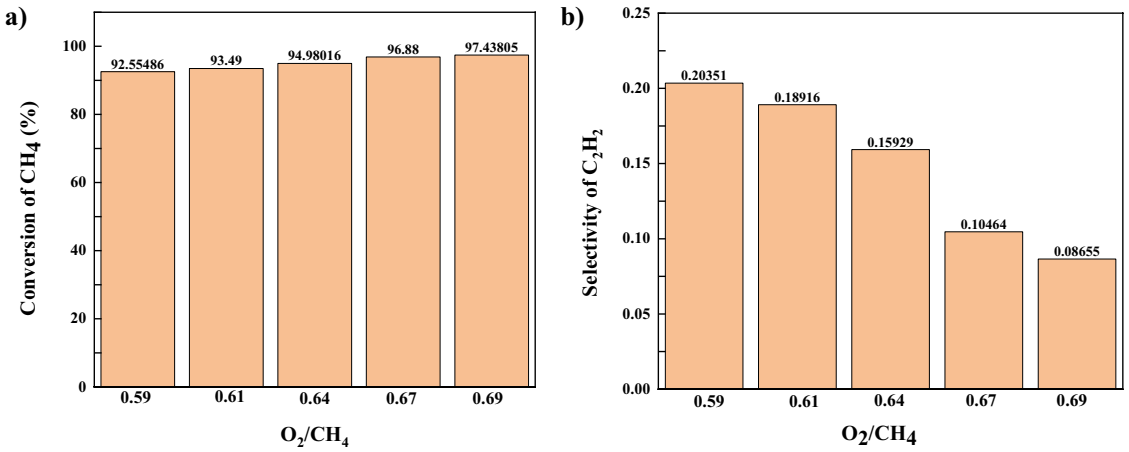

Fig. 14 The effect of increasing the O_2/CH_4 ratio on **a** the percentage conversion of CH_4, **b** the selectivity of C_2H_2

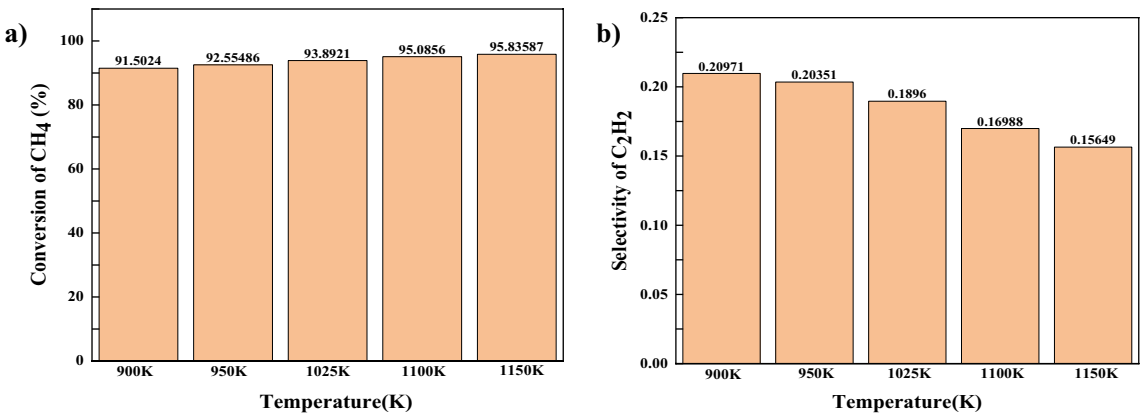

Fig. 15 The effect of increasing the preheating temperature on **a** the conversion of CH_4, **b** the selectivity of C_2H_2

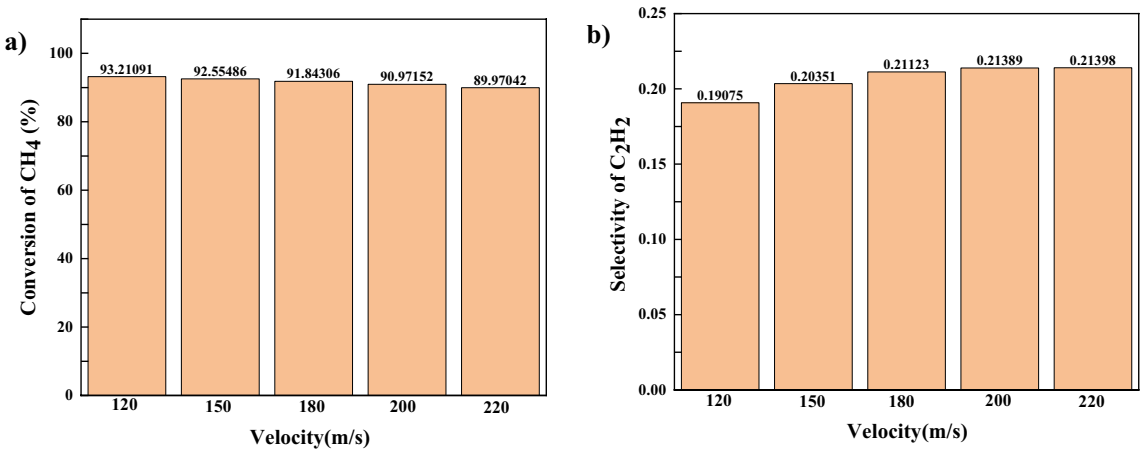

Fig. 16 The effect of increasing the inlet velocity on **a** the conversion of CH_4, **b** the selectivity of C_2H_2

shows that the selectivity of C_2H_2 has been increasing from 0.19075 to 0.21398 by increasing the inlet velocity from 120 to 220 m/s. This suggests that the production of reaction pathways leading to the formation of C_2H_2 has been promoted by increasing the reaction rate. However, the reduction in CH_4 conversion efficiency at higher rates might hinder the rise in selectivity.

Analysis of Variance (AVOVA)

The Analysis of Variance (ANOVA) method is commonly used to determine the important parameters that influence the responses. This is achieved by dividing the total variance into appropriate components and measuring the relative effect of each of them. The *F*-ratio is the ratio of the mean square error to residual error and is often used to determine the importance of a parameter. A high *F*-ratio value for a parameter indicates its high significance, while a lower *p*-value for a parameter suggests greater importance and impact.

Analysis for the Conversion of CH_4

Table 3 presents the results of the analysis of variance for the conversion of CH_4 response. The model's *F*-value is 106.22, and its *p*-value is less than 0.0001, indicating a high degree of accuracy and suitability of the model. The parameters examined in the study are A, B, and C, which represent the preheating temperature, inlet velocity, and the O_2/CH_4 ratio, respectively.

The analysis reveals that the O_2/CH_4 ratio has the most significant impact on the response. Based on the results obtained from the software, Eq. (10) presents the model based on the actual values of each parameter level for the conversion of CH_4. The 2FI model obtained demonstrates the effects of the design parameters on the response in 3D graphs of the response surface.

Table 3 ANOVA for the model of the conversion of CH_4

Source	Sum of squares	*df*	Mean square	*F* value	*p* value	
Model	52.60	6	8.77	106.22	< 0.0001	Significant
A: preheating temperature	15.46	1	15.46	187.27	< 0.0001	
B: velocity	4.01	1	4.01	48.64	0.0001	
C: O_2/CH_4	31.94	1	31.94	387.02	< 0.0001	
AB	0.1301	1	0.1301	1.58	0.2448	
AC	0.7442	1	0.7442	9.02	0.0170	
BC	0.3121	1	0.3121	3.78	0.0878	
Residual	0.6603	8	0.0825			
Cor total	53.26	14				

The high values of $\mathbf{R^2}$ (0.9876) and Adjusted $\mathbf{R^2}$ (0.9783) obtained illustrate the acceptable correlation between the recorded and the predicted response values. Also the agreement between **Predicted** $\mathbf{R^2}$ is 0.9433 and **Adjusted** $\mathbf{R^2}$ is 0.9783, which is a reasonable value and indicates sufficient accuracy

$$\text{Conversion of } CH_4 = -8.05887 + 0.092440 * \text{preheating temperature} - 0.173280 * \text{velocity} + 157.00572 * O_2/CH_4 + 0.000045 \text{ preheating temperature} * \text{velocity} \quad (10)$$

The positive sign in the Eq. (10) indicates an increasing effect of the parameters on the response variable, while the negative sign indicates a decreasing effect. In this equation, all variables have been fully utilized, and the effect of none of the variables has been removed. By drawing a contour diagram, the Design-Expert software enables the examination of the simultaneous effect of variables. Figure 17 illustrates the effect of input parameters on the conversion of CH_4 in a pairwise manner. Based on Fig. 17a, it can be concluded that the preheating temperature has a greater effect than the inlet velocity. On the other hand, Fig. 17b and c demonstrate that the O_2/CH_4 ratio has a greater impact than the inlet velocity and preheating temperature.

According to the normal probability diagram (Fig. 18), the points follow an almost linear pattern, indicating a normal distribution of errors with minimal deviations from linearity. As a result, the model's validity improves when the graph deviates less from linearity and the S-shaped states are reduced.

In Fig. 19, the values of the conversion of CH_4 from the model are compared to those obtained from the experiment, indicating a very good correlation between the two. As shown, all points align along a straight line at a 45° angle, indicating a high level of accuracy in the predictions made by the statistical method.

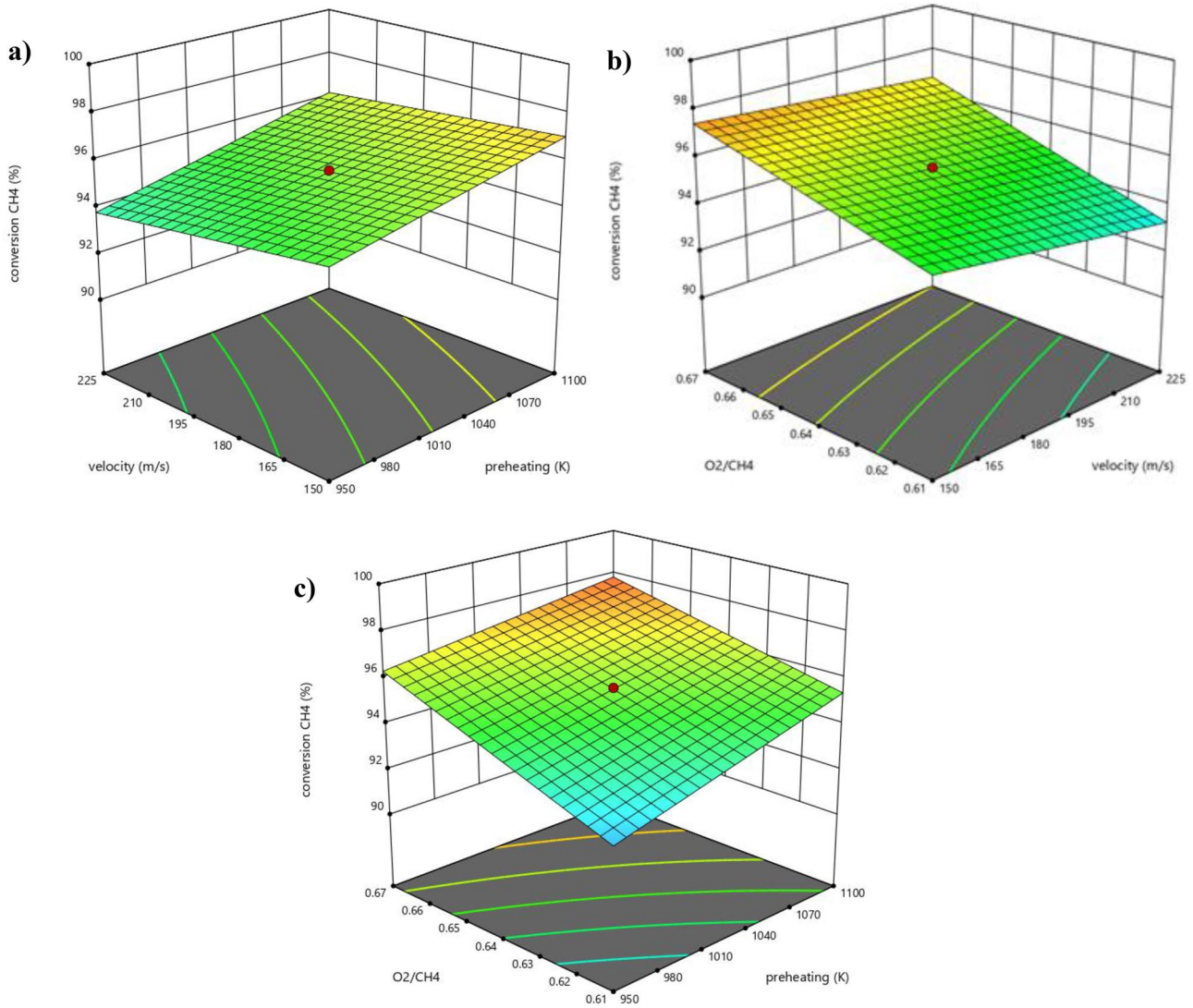

Fig. 17 Combined effect of input parameters **a** velocity. Preheating temperature, **b** O_2/CH_4 velocity and **c** O_2/CH_4 preheating temperature on the conversion of CH_4

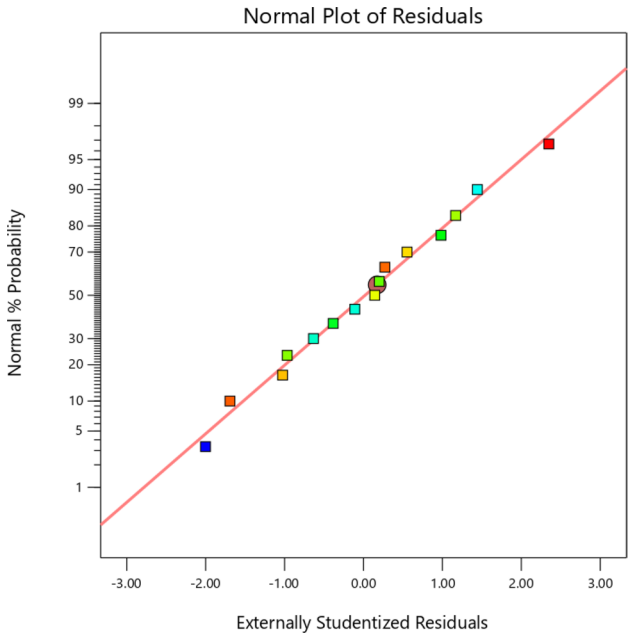

Fig. 18 The normal plot of residuals of the conversion of CH_4

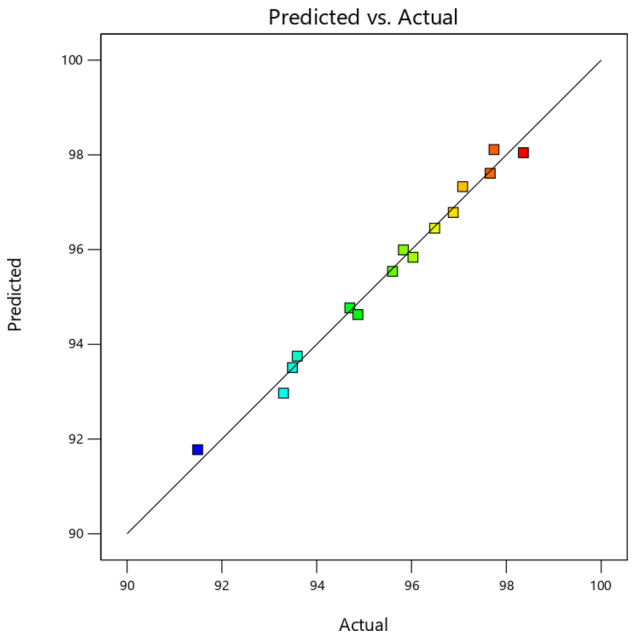

Fig. 19 Predicted vs actual graph of the conversion of CH_4

Analysis for the Selectivity of C_2H_2

The selectivity of C_2H_2 is the next aspect examined in this research. As presented in the Table 4, the satisfactory values of *p*-value and *F*-value demonstrate the high accuracy and fit of the chosen linear model.

The Eq. (11) was chosen using a Power transfer function with a Lambda value of 1.72.

$$\left(\text{Selectivity } C_2H_2\right)^{1.72} = 0.463783 - 0.000109 * \text{preheating temperature} + 0.000175 * \text{velocity} - 0.542377 * O_2/CH_4 \quad (11)$$

The selectivity of C_2H_2 was assessed using a 3D response diagram that considered two parameters: preheating temperature and inlet velocity (Fig. 20). As the inlet velocity in the reactor increases, the selectivity of C_2H_2 also increases since the reaction proceeds in the direction of producing more acetylene. However, the graph indicates that the preheating temperature has a minimal effect on the selectivity of C_2H_2.

The normal probability diagram (Fig. 21) reveals an almost linear trend among the points. This linearity, combined with the uniform distribution, suggests that errors are normally distributed. As a result, this suggests that errors are less frequent.

Figure 22 clearly indicates a significant correspondence between the actual results and the values predicted. The arrangement of all data points in a straight line at a 45° angle is readily observable.

Optimization

In this section, the focus is on optimizing three crucial operating parameters—the O_2/CH_4 ratio, preheating temperature, and velocity of inlet feed. These parameters play a critical role in acetylene production, and the goal is to determine the optimal combination that yields the highest selectivity of C_2H_2 and the highest conversion of CH_4. The optimization function is a useful tool for determining the optimal operating parameters for a given process. In this study, the RSM optimization technique is based on a parameter called "desirability". The desirability function represents an objective measure that varies from zero outside of the limits to one at the goal. By conducting numerical optimization, a point is identified where the desirability function reaches its maximum value.

The Design-Expert software was utilized to optimize the factors by defining the maximum value of acetylene selectivity as the target using the optimization option. The goal was to achieve the maximum value of acetylene selectivity. Table 2 showed that the range of methane conversion is between 0.91 and 0.98. Additionally, higher methane conversion rates are typically associated with lower acetylene selectivity. In natural gas processing, the acceptable range of methane conversion is typically around 95–98%. This means that 95–98% of the methane in the natural gas feedstock is converted into usable products such as ethylene and acetylene. As a result, the optimal range of 0.95–0.98 was selected for methane conversion. Table 5 presents both the lower and upper limits, as well as the weight and importance of each parameter for optimization.

Table 4 ANOVA for the model of the selectivity of C_2H_2

Source	Sum of squares	*df*	Mean square	*F* value	*p* value	
Model	0.0051	3	0.0017	295.91	< 0.0001	Significant
A: preheating temperature	0.0009	1	0.0009	157.54	< 0.0001	
B: velocity	0.0006	1	0.0006	101.09	< 0.0001	
C: O_2/CH_4	0.0036	1	0.0036	628.10	< 0.0001	
Residual	0.0001	11	5.757e−06			
Cor total	0.0052	14				

The high values of $\mathbf{R^2}$ (0.9878) and Adjusted $\mathbf{R^2}$ (0.9844) obtained illustrate the acceptable correlation between the recorded and the predicted response values. Also the agreement between **Predicted** $\mathbf{R^2}$ is 0.9778 and **Adjusted** $\mathbf{R^2}$ is 0.9844, which is a reasonable value and indicates sufficient accuracy

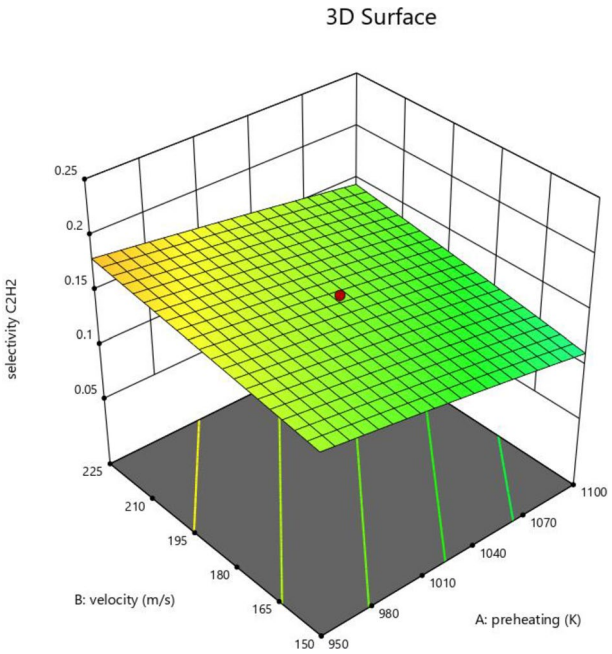

Fig. 20 3D graphs of the geometrical parameters on the selectivity of C_2H_2

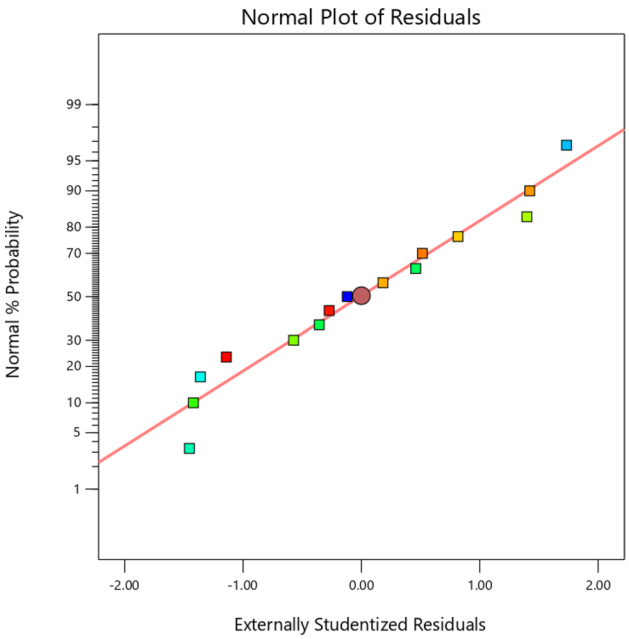

Fig. 21 The normal plot of residuals of the selectivity of C_2H_2

Simultaneous optimization requires assigning low and high values to each goal for every response.

By utilizing optimization and analyzing the data presented in Table 6, the optimal final values for preheating temperature factors, O_2/CH_4 ratio and, inlet velocity have been determined to be 1151.1 K, 0.59, and 222.8 m/s, respectively. Furthermore, the highest acetylene selectivity of 0.191 has been achieved at 95% conversion of CH_4.

To validate the optimal results, simulations were conducted using the optimized values. Table 7 shows a comparison of the results obtained from the simulations and the optimization values, indicating that there is a minimal difference between them.

Conclusion

This study involved conducting 15 CFD experiments, which were created by CCD with five levels of process parameters, in order to examine the conversion of CH_4 and the selectivity for C_2H_2. Process parameters considered are: preheating temperature, inlet velocity and, O_2/CH_4 ratio. Response models were developed for the conversion of CH_4 and the selectivity of C_2H_2 during experiments. Finally, optimization was performed to maximize the selectivity of C_2H_2 for better productivity in the reactor POX methane. The above-mentioned research leads to the following conclusions:

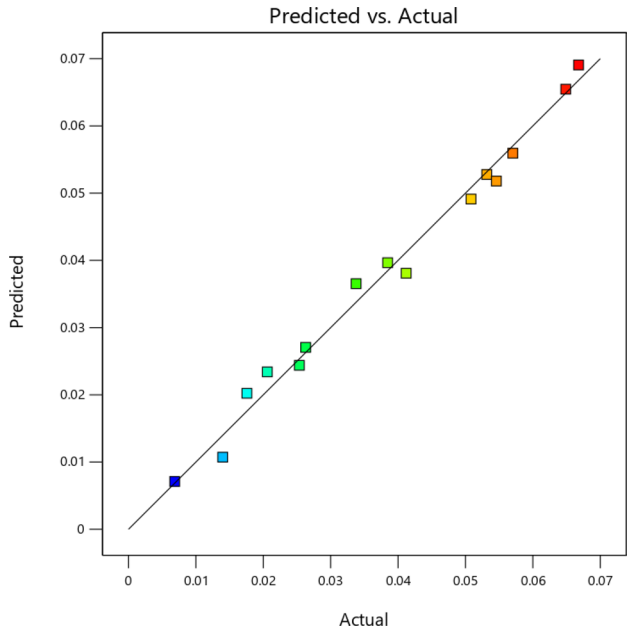

Fig. 22 Predicted vs actual graph of the Selectivity of C_2H_2

(1) Based on the CCD method, the 2FI model for the conversion of CH_4 and Linear model for the selectivity of C_2H_2 were successfully established. The effective parameters of the 2FI model and Linear model were determined by ANOVA, and the accuracy of the model was also explained.

Table 7 Comparison of simulation and optimization results

Response	Simulation	Optimization	Error (%)
Conversion of CH_4 (%)	94.9	95	0.105
Selectivity of C_2H_2	0.186	0.191	2.4

(2) When the preheating temperature rises, the conversion of CH_4 also increases, and the same effect can be observed with O_2/CH_4. But, the conversion of CH_4 experiences a notable decline when the inlet velocity is increased. Furthermore, the selectivity of C_2H_2 exhibits an inverse trend when compared to the conversion of methane.

(3) The optimization for the maximization of the selectivity of C_2H_2 was done using a response surface desirability function. Optimal process parameters were found as preheating temperature, 1151.13 K, inlet velocity, 222.8 m/s, and O_2/CH_4 ratio, 0.59, and corresponding output response as the selectivity of C_2H_2, 0.191 with a desirability of 0.852. Additionally, to verify the output responses, validation experiments were conducted using the optimal preparation parameters. The discrepancy between the experimental measurements and the RSM optimized values for the selectivity of C_2H_2 and the conversion of CH_4 were 2.4% and 0.105%, respectively.

Table 5 Optimization of the selectivity of C_2H_2 by RSM

Name	Goal	Lower limit	Upper limit	Weight	Importance
A: preheating temperature	Is in range	898.85	1151.15	1	3
B: velocity	Is in range	124.425	250.575	1	3
C: O_2/CH_4	Is in range	0.58954	0.69046	1	3
Conversion of CH4	Is in range	95	98.36	1	5
Selectivity of C_2H_2	Maximize	0.0551975	0.207343	1	5

Table 6 Proposed cases by CCD for the optimized operating factors

Case number	Preheating temperature	Velocity	O_2/CH_4	Conversion of CH_4 (%)	Selectivity of C_2H_2	Desirability	Best design
1	1151.13	222.8	0.59	95	0.191	0.852	✓
2	1151.10	222.8	0.59	95.002	0.191	0.852	
3	1151.15	222.8	0.59	95	0.191	0.851	
4	1151.15	222.8	0.59	95	0.191	0.851	
5	1151.40	222.8	0.591	95	0.191	0.851	
6	1151.15	222.8	0.59	95	0.191	0.849	
7	1149.674	222.8	0.59	95.002	0.190	0.849	
8	1151.15	222.8	0.59	95.021	0.190	0.849	
9	1151.1	222.8	0.591	95	0.190	0.848	
10	1151.149	222.8	0.592	95	0.190	0.847	

Overall, the combination of CCD and CFD modeling can serve as a powerful means to investigate various operational states and geometric aspects of reactors in order to optimize their performance, all while requiring only moderate computing resources.

Acknowledgements The authors acknowledge the funding support of Babol Noshirvani University of Technology through Grant Program No. BNUT/388003/99. The authors would like to express their gratitude to the National Iranian Gas Company for providing financial support.

Data availability The data that support the findings of this study are available from the corresponding author upon reasonable request.

References

1. C. Yen, Process Economics Program (PEP) Report 16A: Acetylene SRI Consulting, California (1981)
2. P. Pässler et al., Acetylene. Ullmann's Encyclopedia of Industrial Chemistry **7** (2008)
3. Chemicals from Acetylene. July 2007, Nexant.
4. S. Cao, D. Wang, T. Wang, Simulation of partial oxidation of natural gas with detailed chemistry: influence of addition of H_2, C_2H_6 and C_3H_8. Chem. Eng. Sci. **65**(8), 2608–2618 (2010)
5. W. Zhifang, D. Zheng, Exergy analysis and retrofitting of natural gas-based acetylene process. Chin. J. Chem. Eng. **16**(5), 812–818 (2008)
6. V.Y. Basevich, S. Kogarko, Kinetics of acetylene formation in combustion of methane-oxygen mixtures. Combust. Explos. Shock Waves **14**(1), 35–40 (1978)
7. V. Simonov et al., Development of an algorithm for calculating the parameters of a drum reactor for low-temperature carbonization of oil shale with ash-based heat-transfer agent. Chem. Pet. Eng. **52**, 675–681 (2017)
8. A. Mrakin, G. Akimova, Complex analysis of the efficiency of plants for the thermochemical conversion of solid fuel. Solid Fuel Chem. **49**(4), 261–265 (2015)
9. X. Ku, T. Li, T. Løvås, CFD–DEM simulation of biomass gasification with steam in a fluidized bed reactor. Chem. Eng. Sci. **122**, 270–283 (2015)
10. M.B. Luong et al., Direct numerical simulations of the ignition of lean primary reference fuel/air mixtures with temperature inhomogeneities. Combust. Flame **160**(10), 2038–2047 (2013)
11. C. Bekdemir, B. Somers, P. de Goey, DNS with detailed and tabulated chemistry of engine relevant igniting systems. Combust. Flame **161**(1), 210–221 (2014)
12. B. Franzelli et al., Large eddy simulation of combustion instabilities in a lean partially premixed swirled flame. Combust. Flame **159**(2), 621–637 (2012)
13. D.H. Rowinski, S.B. Pope, Computational study of lean premixed turbulent flames using RANSPDF and LESPDF methods. Combust. Theor. Model. **17**(4), 610–656 (2013)
14. R.O. Fox, *Computational Models for Turbulent Reacting Flows* (Cambridge University Press, Cambridge, 2003)
15. D. Haworth, S. Pope, Transported probability density function methods for Reynolds-averaged and large-eddy simulations. In *Turbulent Combustion Modeling: Advances, New Trends and Perspectives* (2011), pp. 119–142.
16. G.D. Stefanidis et al., CFD simulations of steam cracking furnaces using detailed combustion mechanisms. Comput. Chem. Eng. **30**(4), 635–649 (2006)
17. M. Rehm, P. Seifert, B. Meyer, Theoretical and numerical investigation on the EDC-model for turbulence–chemistry interaction at gasification conditions. Comput. Chem. Eng. **33**(2), 402–407 (2009)
18. S.R. Shabanian et al., Computational fluid dynamics modeling of hydrogen production in an autothermal reactor: effect of different thermal conditions. Korean J. Chem. Eng. **29**, 1531–1540 (2012)
19. M. Evans, P. Medwell, Z. Tian, Modeling lifted jet flames in a heated coflow using an optimized eddy dissipation concept model. Combust. Sci. Technol. **187**(7), 1093–1109 (2015)
20. A. De et al., Numerical simulation of delft-jet-in-hot-coflow (DJHC) flames using the eddy dissipation concept model for turbulence–chemistry interaction. Flow Turbul. Combust. **87**, 537–567 (2011)
21. Y. Xu et al., Numerical simulation of natural gas non-catalytic partial oxidation reformer. Int. J. Hydrogen Energy **39**(17), 9149–9157 (2014)
22. Q. Zhang, J. Wang, T. Wang, Enhancing the acetylene yield from methane by decoupling oxidation and pyrolysis reactions: a comparison with the partial oxidation process. Ind. Eng. Chem. Res. **55**(30), 8383–8394 (2016)
23. L. Chen et al., Experimental and numerical study of a two-stage natural gas combustion pyrolysis reactor for acetylene production: the role of delayed mixing. Proc. Combust. Inst. **37**(4), 5715–5722 (2019)
24. X. Zhou, C. Chen, F. Wang, Multi-dimensional modeling of non-catalytic partial oxidation of natural gas in a high pressure reformer. Int. J. Hydrogen Energy **35**(4), 1620–1629 (2010)
25. H. Amirshaghaghi et al., Numerical simulation of methane partial oxidation in the burner and combustion chamber of autothermal reformer. Appl. Math. Model. **34**(9), 2312–2322 (2010)
26. X. Zhou, C. Chen, F. Wang, Modeling of non-catalytic partial oxidation of natural gas under conditions found in industrial reformers. Chem. Eng. Process. **49**(1), 59–64 (2010)
27. S.E. Hosseini, G. Bagheri, M.A. Wahid, Numerical investigation of biogas flameless combustion. Energy Convers. Manag. **81**, 41–50 (2014)
28. S. Shabanian et al., Experimental and numerical analysis of syngas mild combustion. in *XXXIV Meeting of the Italian Section of the Combustion Institute* (2011)
29. S. Jeon, M. Kwon, Y. Kim, Multi-environment PDF modeling for non-catalytic partial oxidation process under MILD oxy-combustion condition. Int. J. Hydrogen Energy **43**(11), 5486–5500 (2018)
30. T. Kertthong, M. Schmid, G. Scheffknecht, Non-catalytic partial oxidation of methane in biomass-derived syngas with high steam and hydrogen content optimal for subsequent synthesis process. J. Energy Inst. **105**, 251–261 (2022)
31. M.S. Lim, M.S. Hong, Y.N. Chun, Production of synthesis gas from methane using compression ignition reformer. Korean J. Chem. Eng. **26**, 1022–1027 (2009)
32. Z. Liu et al., Investigation of a novel combustion stabilization mechanism and combustion characteristics of a multi-nozzle array model combustor. Fuel **327**, 125138 (2022)
33. A. Gholizadeh et al., Effect of steam addition and distance between inlet nozzles on non-catalytic POX process under MILD combustion condition. Int. J. Hydrogen Energy **47**(1), 127–150 (2022)
34. Q. Peng et al., Effects analysis on combustion and thermal performance enhancement of a nozzle-inlet micro tube fueled by the premixed hydrogen/air. Energy **160**, 349–360 (2018)
35. Y. Tu et al., Effects of furnace chamber shape on the MILD combustion of natural gas. Appl. Therm. Eng. **76**, 64–75 (2015)
36. Z. Wang et al., Experimental study on the effect of combustor configuration on the performance of dual-mode combustor. Aerosp. Sci. Technol. **42**, 169–175 (2015)

37. X. Deng et al., Numerical study of the effect of nozzle configurations on characteristics of MILD combustion for gas turbine application. J. Energy Resour. Technol. (2016). https://doi.org/10.1115/1.4033141
38. W. Zuo et al., Numerical investigations on combustion characteristics of H_2/air premixed combustion in a micro elliptical tube combustor. Energy **126**, 1–12 (2017)
39. T. Förster et al., 3D numerical study of the performance of different burner concepts for the high-pressure non-catalytic natural gas reforming based on the Freiberg semi-industrial test facility HP POX. Fuel **203**, 954–963 (2017)
40. J.A. Mendoza, S. Hwang, Tubular reactor design for the oxidative dehydrogenation of butene using computational fluid dynamics (CFD) modeling. Korean J. Chem. Eng. **35**, 2157–2163 (2018)
41. M. Chmielewski, M. Gieras, Impact of variable geometry combustor on performance and emissions from miniature gas turbine engine. J. Energy Inst. **90**(2), 257–264 (2017)
42. K.-P. Cheong et al., Stability and emission characteristics of non-premixed MILD combustion from a parallel-jet burner in a cylindrical furnace. Energy **170**, 1181–1190 (2019)
43. D. Chen et al., Structural design and performance evaluation of industrial-scale C_2H_2 reactor by partial oxidation of natural gas. Chem. Eng. J. **426**, 130871 (2021)
44. M. Wang et al., Numerical simulation on the emission of NO_x from the combustion of natural gas in the sidewall burner. Therm. Sci. **26**(1 Part A), 247–258 (2022)
45. D. Wang et al., Effects of combustion chamber shapes on combustion and emission characteristics for the n-octanol fueled compression ignition engine. J. Energy Eng. **148**(3), 04022011 (2022)
46. S. Biabani, S.R. Shabanian, H. Bakhshi, CFD study on influence of O_2/CO_2, O_2/H_2O atmospheres and shape of furnace on methane MILD combustion. Int. J. Thermophys. **44**(3), 38 (2023)
47. K. Hamid, S. Vahideh, K. Hami, Combined application of computational fluid dynamics (CFD) and design of experiments (DOE) to hydrodynamic simulation of a coal classifier. Int. J. Min. Geo-Eng. **51**(1), 9–24 (2017)
48. J.O.B. Lira et al., CFD + DoE optimization of a flat plate photocatalytic reactor applied to NO_x abatement. Chem. Eng. Process. Process Intensif. **154**, 107998 (2020)
49. J. Rahmannezhad, S.A. Mirbozorgi, CFD analysis and RSM-based design optimization of novel grooved micromixers with obstructions. Int. J. Heat Mass Transf. **140**, 483–497 (2019)
50. J. Ortega-Casanova, Application of CFD on the optimization by response surface methodology of a micromixing unit and its use as a chemical microreactor. Chem. Eng. Process. Process Intensif. **117**, 18–26 (2017)
51. R.S. Vinod Kumar Srinivasa, B. Shome, Design of experiments enabled CFD approach for optimizing cooling fan performance. SAE Technical Paper (2014). 2014-01-0658
52. J. Kumar, A. Bansal, Photocatalytic degradation in annular reactor: modelization and optimization using computational fluid dynamics (CFD) and response surface methodology (RSM). J. Environ. Chem. Eng. **1**(3), 398–405 (2013)
53. T. Canonsburg, ANSYS fluent user's guide. ANSYS FLUENT User's Guide **15317**, 2498 (2017)
54. Q. Zhang et al., Simulations of methane partial oxidation by CFD coupled with detailed chemistry at industrial operating conditions. Chem. Eng. Sci. **142**, 126–136 (2016)
55. G.P. Smith, D.M. Golden, M. Frenklach, N.W. Moriarty, B. Eiteneer, M. Goldenberg, T.C. Bowman, R.K. Hanson, S. Song, W.C. Gardiner Jr., V.V. Lissianski, Z. Qin (2013), https://www.me.berkeley.edu/gri-mech/. Accessed 1 Oct 2013
56. S.R. Shabanian et al., Kinetic and fluid dynamic modeling of ethylene jet flames in diluted and heated oxidant stream combustion conditions. Appl. Therm. Eng. **52**(2), 538–554 (2013)
57. J. Lawson, *Design and Analysis of Experiments with R*, vol. 115 (CRC Press, Boca Raton, 2014)
58. G.E. Box, J.S. Hunter, Multi-factor experimental designs for exploring response surfaces. Ann. Math. Stat. **28**, 195–241 (1957)
59. X. Sun et al., Multi-objective optimization of a Stairmand cyclone separator using response surface methodology and computational fluid dynamics. Powder Technol. **320**, 51–65 (2017)